

Vector Approximate Message Passing based Channel Estimation for MIMO-OFDM Underwater Acoustic Communications

Wenxuan Chen, Jun Tao, *Senior Member, IEEE*, Lu Ma, *Member, IEEE*,

and Gang Qiao, *Member, IEEE*

Abstract

Accurate channel estimation is critical to the performance of orthogonal frequency-division multiplexing (OFDM) underwater acoustic (UWA) communications, especially under multiple-input multiple-output (MIMO) scenarios. In this paper, we explore Vector Approximate Message Passing (VAMP) coupled with Expected Maximum (EM) to obtain channel estimation (CE) for MIMO OFDM UWA communications. The EM-VAMP-CE scheme is developed by employing a Bernoulli-Gaussian (BG) prior distribution for the channel impulse response, and hyperparameters of the BG prior distribution are learned via the EM algorithm. Performance of the EM-VAMP-CE is evaluated through both synthesized data and real data collected in two at-sea UWA communication experiments. It is shown the EM-VAMP-CE achieves better performance-complexity tradeoff compared with existing channel estimation methods.

Index Terms

Channel Estimation (CE), Multiple-Input Multiple-Output (MIMO), Orthogonal Frequency-Division Multiplexing (OFDM), Underwater Acoustic (UWA) Communications, Vector Approximate Message Passing (VAMP).

I. INTRODUCTION

Due to its limited bandwidth, multipath fading, and significant Doppler effect, the underwater acoustic (UWA) channel has long been recognized as one of the most challenging communication media [1].

W. Chen and J. Tao are with the Key Laboratory of Underwater Acoustic Signal Processing of the Ministry of Education, School of Information Science and Engineering, Southeast University, Nanjing, 210096, China. L. Ma and G. Qiao are with the Acoustic Science and Technology Laboratory, the Key Laboratory of Marine Information Acquisition and Security, Ministry of Industry and Information Technology, and the College of Underwater Acoustic Engineering, Harbin Engineering University, Harbin, 150001, China. (Email: jtao@seu.edu.cn)

Attributed to the progress in Doppler compensation, orthogonal frequency-division multiplexing (OFDM) modulation is receiving many attentions in UWA communication, for its immunity to multipath propagation, high spectral efficiency, and so on. The channel estimation (CE) is one of key factors in the performance of OFDM UWA communications [2], [3].

Conventional least squares (LS) and linear minimum mean square error (LMMSE) channel estimations are found in OFDM UWA communications [1], [4]–[7]. Even though, an underwater acoustic channel generally has a long delay spread, making aforementioned traditional methods inefficient in the sense that a large pilot overhead is required [1], [5]. UWA channels usually manifest sparse property, meaning that a large percentage of channel energy is concentrated at a small amount of taps. This observation naturally motivates the development of sparsity-aware channel estimation so as to reduce pilot overhead and/or complexity. Initial effort was found in single-carrier UWA communications [8], where compressive sensing (CS) algorithms including matching pursuit (MP), orthogonal matching pursuit (OMP), etc. were employed to achieve channel estimation. The development of sparsity-aware channel estimations for OFDM UWA communications can be found in [9]–[13], again mainly attributed to the CS techniques. In [9]–[11], the greedy OMP algorithm and its variants were used. In [9], block fast Fourier transform (FFT) was adopted to reduce the implementation complexity of OMP channel estimation. In [10], the OMP algorithm was employed for joint channel estimation and impulsive noise mitigation in OFDM underwater acoustic communications. In [11], channel estimation for OFDM UWA communications was achieved via adaptive OMP (A-OMP) algorithm, which outperforms standard OMP method for improved termination condition. In [12], [13], convex-optimization-type CS methods including Basis Pursuit (BP) and Basis Pursuit denoising (BPDN) were adopted. In [12], three implementations of BP, named the l_1 _ls, SpaRSA, and YALL1, were used for estimating time-varying sparse channels. Simulation and experimental results showed they were comparable in performance, but the SpaRSA and YALL1 had lower complexity. In [13], a BPDN-based channel estimation was proposed for OFDM UWA communications employing virtual time reversal processing. It slightly outperformed the channel estimation via MP algorithm. In [14], channel estimations based on subspace methods ESPRIT and Root-MUSIC as well as CS algorithms including OMP and BP, were investigated and compared for OFDM UWA communications under different Doppler conditions. A path-based channel model was adopted, that is the channel is described by a limited number of paths, each characterized by a delay, Doppler scale, and attenuation factor. It showed the CS based CE has better performance than the subspace based CE, and the BP-CE slightly outperforms the OMP-CE.

Bayesian inference techniques like the maximum a posteriori probability (MAP) estimation, sparse Bayesian learning (SBL) algorithm [15], [16], and approximate message passing (AMP) techniques [17], [18] and variants, have found success in terrestrial OFDM systems [19]–[21]. Due to the improved performance and robustness, they have also attracted many attentions in OFDM UWA systems [22]–[25] recently. In [22], an OMP-MAP algorithm was proposed for OFDM UWA channel estimation. With the path delays and Doppler spread identified via OMP, path gains were estimated using the MAP technique. The OMP-MAP channel estimation outperforms conventional OMP CE. In [23], an SBL based channel estimation scheme was proposed for OFDM UWA communications. To further improve the performance, temporal correlation in channels across consecutive OFDM blocks was utilized, leading to the so-called temporal multiple SBL (TMSBL) channel estimator. In [24], the SBL was employed for the joint estimation and tracking of channel and impulsive noise in OFDM UWA systems. Compared with traditional SBL estimation, this work exploited the joint sparsity of channel and impulse noise for better estimation performance.

Despite decent performance, the SBL-CE and MAP-CE often suffer high computation complexity, which limits their practical applications [26], [27]. In contrast, the AMP-type techniques have the advantage of lower complexity [28], [29]. The generalized AMP (GAMP) [30] as a generalization of AMP [17], has been used for channel estimation in OFDM UWA communications suffering impulsive noise [25]. The GAMP, however, works well only when the measurement matrix consists of independent and identically distributed (i.i.d.) Gaussian elements. Therefore, its practical application is limited. Recently, the vector AMP (VAMP) algorithm was proposed [31], [32]. It is applicable to a wider class of right-rotationally invariant measurement matrices. In light of this, we have made a preliminary investigation on the feasibility of VAMP based channel estimation for OFDM UWA communication systems [?]. In this paper, a much more comprehensive study on the VAMP based channel estimation was presented for multiple-input multiple-output (MIMO) OFDM UWA communication system. The Bernoulli-Gaussian (BG) prior distribution is adopted for the UWA channel to account for its sparsity. Parameters of the BG distribution are learned from the received data via the Expectation Maximization (EM) algorithm, instead of being set empirically as in [?]. The complexity of the resulting EM-VAMP-CE was analyzed and compared with existing LS, LMMSE, OMP, and SBL CEs, under scenarios of non-orthogonal pilot sequences and orthogonal pilot sequences. It showed the complexity of the EM-VAMP-CE is significantly lower than that of the SBL-CE when non-orthogonal pilot sequences were employed. To verify the performance of

the EM-VAMP-CE, MIMO OFDM UWA communication systems employing overlapping pilot pattern across transducers [1] were considered. Both synthesized data and real data were used for verification. In the simulation, orthogonal pilot sequences [33] were adopted. The real data were collected in two UWA communication experiments: XM16 and SPACE08, where non-orthogonal pilot sequences were adopted. For comparison purpose, channel estimations based on LS, LMMSE, OMP, and SBL were also included. Both simulation and experimental results show the proposed EM-VAMP-CE achieves the best performance-complexity tradeoff at a low pilot overhead.

The rest of this paper is organized as follows. In Section II, the system model for zero-padding (ZP) MIMO OFDM UWA communications is presented. In Section III, the EM-VAMP based channel estimator is derived. Section IV and Section V present simulation and experimental results, respectively. Section VI concludes this paper.

Notation: The $\mathcal{C}^{p \times q}$ represents a complex space of dimension $p \times q$. The superscripts $(\cdot)^T$ and $(\cdot)^H$ represent the transpose and Hermitian, respectively. The \odot denotes the Hadamard product. The $\langle \cdot \rangle$ is an empirical averaging operation defined as $\langle \mathbf{x} \rangle = \frac{1}{P} \sum_{p=1}^P x_p$, where x_p is the p -th element of the size- P vector \mathbf{x} . The $\text{Diag}(\mathbf{a})$ represents a diagonal matrix with the vector \mathbf{a} on its diagonal. The $\mathbb{E}[\cdot]$ denotes an expectation operation and the $\text{Tr}[\cdot]$ takes the trace of a matrix. The $\|\cdot\|_F$ represents the Frobenius norm, and the \mathbf{I} is an identity matrix. The $\mathcal{CN}(x; \mu, \sigma^2) \triangleq \frac{1}{\pi\sigma^2} \exp\left(\frac{-|x-\mu|^2}{\sigma^2}\right)$ is the probability density function of a circularly symmetric complex Gaussian distribution with mean μ and variance σ^2 . The \mathbf{F}_K denotes a size- K normalized DFT matrix with its (m, n) -th element being $w_{m,n} = \frac{1}{\sqrt{K}} e^{-j2\pi \frac{mn}{K}}$ for $m, n = 0, 1, \dots, K-1$. The $\delta(\cdot)$ is a Dirac delta function.

II. SYSTEM MODEL

An MIMO OFDM UWA communication system with N transducers and M hydrophones is considered. To maintain a high transmission efficiency, the same pilot subcarrier index set, $\mathcal{P} = [I_1, I_2, \dots, I_{K_p}]$, is employed across all transducers. In addition to the K_p pilot symbols, each OFDM block carries K_d data symbols, resulting in a block length of $K = K_p + K_d$ [1]. On the n -th transducer, a block of pilot/data symbols $\mathbf{X}_n = [X_n(0), X_n(1), \dots, X_n(K-1)]^T$ are modulated onto different subcarriers through an inverse discrete Fourier transform (IDFT) operation, leading to the time-domain OFDM symbol $\mathbf{x}_n = \mathbf{F}_K^H \mathbf{X}_n = [x_n(0), x_n(1), \dots, x_n(K-1)]^T$. In order to eliminate the inter-block interference (IBI), a guard interval in form of zero-padding is added at the end of \mathbf{x}_n . The length of the guard interval is chosen as $N_{ZP} \geq L$, with L being the channel length [34].

On the receiver side, Doppler preprocessing via resampling and carrier frequency offset (CFO) compensation is first performed, such that the channel can be treated time-invariant over one OFDM block [1]. On the m -th hydrophone, the received signal at time k is then represented as

$$\underline{y}_m(k) = \sum_{n=1}^N \sum_{l=0}^{L-1} \underline{h}_{m,n}(l) x_n(k-l) + \underline{n}_m(k) \quad (1)$$

where $\underline{h}_{m,n}(l)$ is the l -th tap of the discrete-time subchannel between the n -th transducer and the m -th hydrophone. After performing an overlap-adding (OLA) operation as follows [34]

$$\begin{aligned} \underline{\mathbf{y}}_m = & [\underline{y}_m(0), \underline{y}_m(1), \underline{y}_m(2), \dots, \underline{y}_m(K-1)] \\ & + [\underline{y}_m(K), \dots, \underline{y}_m(K+L-2), 0 \dots, 0] \end{aligned} \quad (2)$$

and a K -point DFT operation, the frequency-domain vector is obtained as $\tilde{\mathbf{y}}_m = \mathbf{F}_K \underline{\mathbf{y}}_m$. For the purpose of channel estimation, the frequency-domain samples corresponding to the K_p pilot subcarriers are extracted out of $\tilde{\mathbf{y}}_m$, leading to $\mathbf{y}_m = [y_{m,I_1}, y_{m,I_2}, \dots, y_{m,I_p}] \in \mathcal{C}^{K_p \times 1}$. The \mathbf{y}_m can be expressed as

$$\mathbf{y}_m = \sum_{n=1}^N \mathbf{S}_n \mathbf{F} \underline{\mathbf{h}}_{m,n} + \mathbf{n}_m = \mathbf{W} \underline{\mathbf{h}}_m + \mathbf{n}_m \quad (3)$$

where $\mathbf{S}_n = \text{Diag}(X_n(I_1), X_n(I_2), \dots, X_n(I_{K_p}))$ is a diagonal matrix consisting of K_p pilot symbols sent by the n -th transducer, $\mathbf{F} \in \mathcal{C}^{K_p \times L}$ is made up of K_p rows with indices given in \mathcal{P} and the first L columns of \mathbf{F}_K , $\mathbf{W} = [\mathbf{S}_1 \mathbf{F}, \mathbf{S}_2 \mathbf{F}, \dots, \mathbf{S}_N \mathbf{F}] \in \mathcal{C}^{K_p \times NL}$. The $\underline{\mathbf{h}}_{m,n} = [\underline{h}_{m,n}(0), \underline{h}_{m,n}(1), \dots, \underline{h}_{m,n}(L-1)]^T \in \mathcal{C}^{L \times 1}$, and $\underline{\mathbf{h}}_m = [\underline{\mathbf{h}}_{m,1}^h, \underline{\mathbf{h}}_{m,2}^h, \dots, \underline{\mathbf{h}}_{m,N}^h]^h \in \mathcal{C}^{NL \times 1}$. The $\mathbf{n}_m \in \mathcal{C}^{K_p \times 1}$ is the frequency-domain noise vector, assumed to follow a complex Gaussian distribution $\mathcal{CN}(\mathbf{0}, \gamma_w^{-1} \mathbf{I})$. It is noted when a path-based channel model [14] is considered, the system model in (3) is still valid if only the Doppler effect can be properly compensated. The goal of channel estimation is to estimate $\underline{\mathbf{h}}_m$ based on (3).

III. EM-VAMP BASED CHANNEL ESTIMATION

The problem given by (3) is a standard linear regression (SLR) problem, which can be solved via the VAMP algorithm. In the following, we first present the VAMP based channel estimation, temporarily assuming model parameters and super-parameters are known. After that, parameter estimation via EM method is introduced. Last, a complexity comparison between the proposed EM-VAMP channel estimation scheme and existing methods is made.

A. VAMP based channel estimation

The VAMP algorithm provides an iterative procedure for approximately solving the MAP or minimum mean-squared error (MMSE) estimation of $\underline{\mathbf{h}}_m$ based on observed data \mathbf{y}_m in (3). In this paper, we seek an MMSE estimation of $\underline{\mathbf{h}}_m$.

We assume $\underline{\mathbf{h}}_m$ has i.i.d elements and to characterize its sparsity, each element follows a Bernoulli-Gaussian prior distribution. Therefore

$$\begin{aligned} p(\underline{\mathbf{h}}_m; \boldsymbol{\theta}_1) &= \prod_{i=1}^{NL} p(\underline{h}_m(i); \boldsymbol{\theta}_1) \\ &= \prod_{i=1}^{NL} (1 - \lambda)\delta(\underline{h}_m(i)) + \lambda\mathcal{CN}(\underline{h}_m(i); 0, \gamma_h^{-1}) \end{aligned} \quad (4)$$

where $\boldsymbol{\theta}_1 = [\lambda, \gamma_h]^T$ contains the hyper-parameters, $\lambda \in (0, 1)$ is the normalized sparsity of the channel, and γ_h denotes the precision (inverse variance) of the distribution of a non-zero channel element. From (3), it is easy to have

$$\begin{aligned} p(\mathbf{y}_m, \underline{\mathbf{h}}_m; \boldsymbol{\theta}) &= p(\underline{\mathbf{h}}_m; \boldsymbol{\theta}_1)p(\mathbf{y}_m|\underline{\mathbf{h}}_m; \boldsymbol{\theta}) \\ &= p(\underline{\mathbf{h}}_m; \boldsymbol{\theta}_1)\mathcal{CN}(\mathbf{y}_m; \mathbf{W}\underline{\mathbf{h}}_m, \gamma_w^{-1}\mathbf{I}) \end{aligned} \quad (5)$$

where $\boldsymbol{\theta} = [\boldsymbol{\theta}_1^T \ \gamma_w]^T$. Splitting $\underline{\mathbf{h}}_m$ into two identical variables $\mathbf{h}_1 = \mathbf{h}_2$ [32], leads to the following equivalent factorization

$$p(\mathbf{y}_m, \mathbf{h}_1, \mathbf{h}_2; \boldsymbol{\theta}) = p(\mathbf{h}_1; \boldsymbol{\theta}_1)\delta(\mathbf{h}_1 - \mathbf{h}_2)\mathcal{CN}(\mathbf{y}_m; \mathbf{W}\mathbf{h}_2, \gamma_w^{-1}\mathbf{I}) \quad (6)$$

A factor graph representation of (6) is given in Fig. 1, where we have two variable nodes (VNs) and one factor node (FN).

It is well known the exact MMSE estimation of $\underline{\mathbf{h}}_m$ is $\hat{\underline{\mathbf{h}}}_m^{\text{MMSE}} = \mathbb{E}[\underline{\mathbf{h}}_m|\mathbf{y}_m]$, which boils down to computing the posterior distribution $p(\underline{\mathbf{h}}_m|\mathbf{y}_m)$. The VAMP provides an iterative way to approximately compute the posterior distribution, as discussed in the following.

In the k -th iteration of the VAMP-based channel estimation, the sum-product (SP) belief [32] (posterior probability) of the VN \mathbf{h}_1 can be computed with the channel prior probability $p(\mathbf{h}_1; \boldsymbol{\theta}_1)$ and the message $\mu_{\delta \rightarrow \mathbf{h}_1}$ in form of $\mathcal{CN}(\mathbf{h}_1; \mathbf{r}_{1,k}, \gamma_{1,k}^{-1}\mathbf{I})$ from the FN δ . Attributed to the i.i.d assumption, it is equivalent

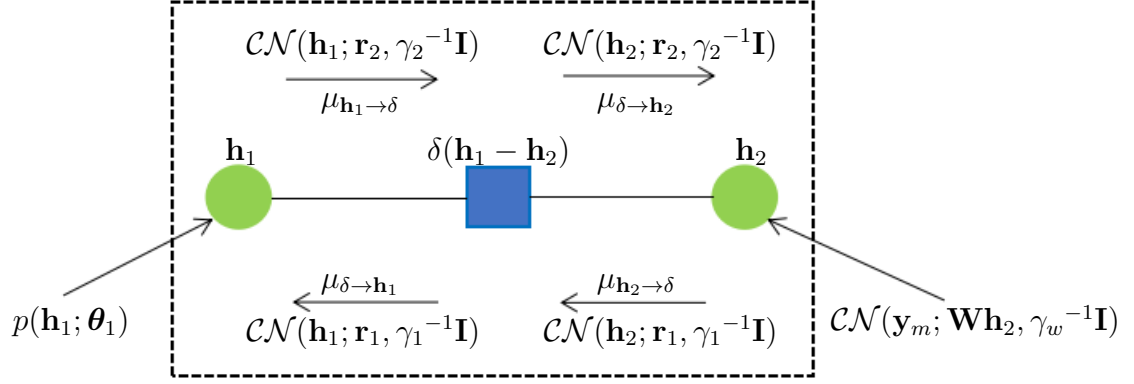


Fig. 1. The factor graph for VAMP channel estimation (the circle and square nodes represent, respectively, a variable node and a factor node).

to compute the SP belief for each of its elements, that is

$$b_1(h_1(i)|r_{1,k}(i), \gamma_{1,k}, \boldsymbol{\theta}_1) = \frac{\mathcal{CN}(h_1(i); r_{1,k}(i), \gamma_{1,k}^{-1})p(h_1(i); \boldsymbol{\theta}_1)}{\int \mathcal{CN}(h_1(i); r_{1,k}(i), \gamma_{1,k}^{-1})p(h_1(i); \boldsymbol{\theta}_1)dh_1(i)} \quad (7)$$

$$= (1 - \pi_k(i))\delta(h_1(i)) + \pi_k(i)\mathcal{CN}(h_1(i); \mu_k(i), \nu_k) \quad (8)$$

where

$$\pi_k(i) = \left(1 + \frac{(1 - \lambda)\mathcal{CN}(0; r_{1,k}(i), \gamma_{1,k}^{-1})}{\lambda\mathcal{CN}(0; r_{1,k}(i), (\gamma_{1,k}^{-1} + \gamma_h^{-1}))}\right)^{-1} \quad (9)$$

$$\mu_k(i) = \frac{\gamma_{1,k}r_{1,k}(i)}{\gamma_{1,k} + \gamma_h} \quad (10)$$

$$\nu_k = \frac{1}{\gamma_{1,k} + \gamma_h} \quad (11)$$

Details are referred to Appendix A. The posteriori mean-vector $\hat{\mathbf{h}}_{1,k}$ and inverse-variance $\eta_{1,k}$ of \mathbf{h}_1 are then obtained as

$$\hat{\mathbf{h}}_{1,k} = \boldsymbol{\pi}_k \odot \boldsymbol{\mu}_k = \boldsymbol{\pi}_k \odot \frac{\gamma_{1,k}\mathbf{r}_{1,k}}{\gamma_{1,k} + \gamma_h} \quad (12)$$

$$\eta_{1,k} = \frac{\gamma_{1,k}}{\alpha_{1,k}} \quad (13)$$

where $\boldsymbol{\pi}_k = [\pi_k(1), \pi_k(2), \dots, \pi_k(NL)]^T$, $\boldsymbol{\mu}_k = [\mu_k(1), \mu_k(2), \dots, \mu_k(NL)]^T$, and

$$\alpha_{1,k} = \left\langle \boldsymbol{\pi}_k \frac{\gamma_{1,k}}{\gamma_{1,k} + \gamma_h} \right\rangle \quad (14)$$

The SP belief of \mathbf{h}_1 is approximated as a complex Gaussian distribution $\mathcal{CN}(\mathbf{h}_1; \hat{\mathbf{h}}_{1,k}, \eta_{1,k}^{-1}\mathbf{I})$, according to the VAMP algorithm. The message to be passed from the VN \mathbf{h}_1 to the FN δ , $\mu_{\mathbf{h}_1 \rightarrow \delta}$, can then be obtained via Gaussian division as $\frac{\mathcal{CN}(\mathbf{h}_1; \hat{\mathbf{h}}_{1,k}, \eta_{1,k}^{-1}\mathbf{I})}{\mathcal{CN}(\mathbf{h}_1; \mathbf{r}_{1,k}, \gamma_{1,k}^{-1}\mathbf{I})} \propto \mathcal{CN}(\mathbf{h}_1; \mathbf{r}_{2,k}, \gamma_{2,k}^{-1}\mathbf{I})$, where

$$\mathbf{r}_{2,k} = \frac{(\hat{\mathbf{h}}_{1,k} - \alpha_{1,k}\mathbf{r}_{1,k})}{1 - \alpha_{1,k}} \quad (15)$$

$$\gamma_{2,k} = \gamma_{1,k} \frac{1 - \alpha_{1,k}}{\alpha_{1,k}} \quad (16)$$

The message $\mu_{\mathbf{h}_1 \rightarrow \delta}$ is forwarded by the FN δ to the VN \mathbf{h}_2 without change, such that $\mu_{\delta \rightarrow \mathbf{h}_2} = \mathcal{CN}(\mathbf{h}_2; \mathbf{r}_{2,k}, \gamma_{2,k}^{-1}\mathbf{I})$. With the message $\mu_{\delta \rightarrow \mathbf{h}_2}$ and the likelihood function $\mathcal{CN}(\mathbf{y}_m; \mathbf{W}\mathbf{h}_2, \gamma_w^{-1}\mathbf{I})$, the SP belief of \mathbf{h}_2 can be evaluated as follows

$$b_2(\mathbf{h}_2 | \mathbf{r}_{2,k}, \gamma_{2,k}, \gamma_w) = \frac{\mathcal{CN}(\mathbf{h}_2; \mathbf{r}_{2,k}, \gamma_{2,k}^{-1}\mathbf{I})p(\mathbf{y}_m | \mathbf{h}_2; \gamma_w)}{\int \mathcal{CN}(\mathbf{h}_2; \mathbf{r}_{2,k}, \gamma_{2,k}^{-1}\mathbf{I})p(\mathbf{y}_m | \mathbf{h}_2; \gamma_w)d\mathbf{h}_2} \quad (17)$$

which is Gaussian with its mean $\hat{\mathbf{h}}_{2,k}$ and covariance matrix \mathbf{D}_k given by

$$\hat{\mathbf{h}}_{2,k} = (\gamma_w \mathbf{W}^H \mathbf{W} + \gamma_{2,k} \mathbf{I})^{-1} (\gamma_w \mathbf{W}^H \mathbf{y}_m + \gamma_{2,k} \mathbf{r}_{2,k}) \quad (18)$$

$$\mathbf{D}_k = (\gamma_w \mathbf{W}^H \mathbf{W} + \gamma_{2,k} \mathbf{I})^{-1} \quad (19)$$

The SP belief of \mathbf{h}_2 is further approximated as complex Gaussian $\mathcal{CN}(\mathbf{h}_2; \hat{\mathbf{h}}_{2,k}, \eta_{2,k}^{-1}\mathbf{I})$, where

$$\eta_{2,k} = \frac{\gamma_{2,k}}{\alpha_{2,k}} \quad (20)$$

$$\alpha_{2,k} = \frac{\gamma_{2,k}}{N} \text{Tr}[\mathbf{D}_k] \quad (21)$$

In (18) and (19), matrix inversion is required. When orthogonal pilot sequences [33] are employed, $\mathbf{W}^H \mathbf{W}$ is diagonal so the matrix inversion only incurs a low complexity. Otherwise, \mathbf{W} can be replaced by its

singular value decomposition (SVD) $\mathbf{W} = \mathbf{U}\mathbf{S}\mathbf{V}^H$ such that (18) and (21) become

$$\widehat{\mathbf{h}}_{2,k} = \mathbf{V}\mathbf{d}_k(\widetilde{\mathbf{y}}_m + \gamma_{2,k}\mathbf{V}^H\mathbf{r}_{2,k}) \quad (22)$$

$$\alpha_{2,k} = \frac{1}{R} \sum_n \frac{\gamma_{2,k}}{\gamma_w s_n^2 + \gamma_{2,k}}, \quad (23)$$

where $R = \text{rank}(\mathbf{W})$, $s_n = [\mathbf{S}]_{nn}$, and

$$\mathbf{d}_k = (\gamma_w \mathbf{S}^H \mathbf{S} + \gamma_{2,k} \mathbf{I})^{-1} \quad (24)$$

$$\widetilde{\mathbf{y}}_m = \gamma_w \mathbf{S}^H \mathbf{y}_m. \quad (25)$$

This completes the message passing from \mathbf{h}_1 to \mathbf{h}_2 . Now, via Gaussian division, the message to be passed from the VN \mathbf{h}_2 to the FN δ , $\mu_{\mathbf{h}_2 \rightarrow \delta}$, can be similarly obtained as

$$\mathbf{r}_{1,k+1} = \frac{(\widehat{\mathbf{h}}_{2,k} - \alpha_{2,k}\mathbf{r}_{2,k})}{1 - \alpha_{2,k}} \quad (26)$$

$$\gamma_{1,k+1} = \gamma_{2,k} \frac{1 - \alpha_{2,k}}{\alpha_{2,k}} \quad (27)$$

where $k + 1$ indicates the message is for the next $(k + 1)$ -th iteration. Convergence of the VAMP-based iterative channel estimation is determined from the normalized difference defined as $\xi_k = \frac{\|\mathbf{r}_{1,k+1} - \mathbf{r}_{1,k}\|_2^2}{\|\mathbf{r}_{1,k+1}\|_2^2}$. We stop the iteration when ξ_k is lower than some predefined threshold ξ_T .

B. Parameter Estimations using the EM Algorithm

The parameter vector $\boldsymbol{\theta} = [\boldsymbol{\theta}_1, \gamma_w]^T$ involved in the VAMP based channel estimation is unknown and has to be estimated in practical use. In this section, we present a parameter estimation scheme based on the EM algorithm. The operation of the EM algorithm is very convenient in light of the use of VAMP for channel estimation, as the posterior probability required in the E step is already available in (7) and (17). The EM algorithm is itself iterative and to maintain a high efficiency, we make the iterations of the EM and VAMP coincide.

We next present the EM based parameter estimation in the k -th iteration. In the E-step, the expectation

of $\ln p(\underline{\mathbf{h}}_m, \mathbf{y}_m | \boldsymbol{\theta})$ is taken with respect to (7) [35], leading to

$$\begin{aligned} Q_1(\boldsymbol{\theta}_1, \boldsymbol{\theta}_{1,k-1}) &= \mathbb{E}[\ln p(\underline{\mathbf{h}}_m, \mathbf{y}_m | \boldsymbol{\theta}) | \mathbf{r}_{1,k}, \gamma_{1,k}, \boldsymbol{\theta}_{1,k-1}] \\ &= \int \ln(p(\underline{\mathbf{h}}_m; \boldsymbol{\theta}_1) p(\mathbf{y}_m | \underline{\mathbf{h}}_m; \gamma_w)) b_1(\underline{\mathbf{h}}_m | \mathbf{r}_{1,k}, \gamma_{1,k}, \boldsymbol{\theta}_{1,k-1}) d\underline{\mathbf{h}}_m, \end{aligned} \quad (28)$$

where $\boldsymbol{\theta}_{1,k-1}$ is the estimation of $\boldsymbol{\theta}_1$ in the $(k-1)$ -th iteration. In the M-step, we seek an optimal parameter estimation, $\boldsymbol{\theta}_{1,k}$, that maximizes (28) as follows

$$\boldsymbol{\theta}_{1,k} = \arg \max_{\boldsymbol{\theta}_1} Q_1(\boldsymbol{\theta}_1, \boldsymbol{\theta}_{1,k-1}) \quad (29)$$

The solution of $\boldsymbol{\theta}_{1,k}$ is obtained as follows

$$\lambda_k = \frac{1}{NL} \sum_{i=1}^{NL} \pi_k(i) \quad (30)$$

$$\gamma_{h,k} = \left(\frac{1}{\lambda_k NL} \sum_{i=1}^{NL} \pi_k(i) (|\mu_k(i)|^2 + \nu_k) \right)^{-1} \quad (31)$$

where $\pi_k(i)$, $\mu_k(i)$, and ν_k are given by (9), (10), (11), respectively. The derivation is referred to Appendix B.

We continue to estimate γ_w by constructing the following cost function in the E-step

$$\begin{aligned} Q_2(\gamma_w, \gamma_{w,k-1}) &= \mathbb{E}[\ln(p(\underline{\mathbf{h}}_m; \boldsymbol{\theta}_1) p(\mathbf{y}_m | \underline{\mathbf{h}}_m; \gamma_w)) | \mathbf{r}_{2,k}, \gamma_{2,k}, \gamma_{w,k-1}] \\ &= \int \ln(p(\underline{\mathbf{h}}_m; \boldsymbol{\theta}_1) p(\mathbf{y}_m | \underline{\mathbf{h}}_m; \gamma_w)) b_2(\underline{\mathbf{h}}_m | \mathbf{r}_{2,k}, \gamma_{2,k}, \gamma_{w,k-1}) d\underline{\mathbf{h}}_m \end{aligned} \quad (32)$$

where $\gamma_{w,k-1}$ is the estimation of γ_w in the $(k-1)$ -th iteration. In the M-step, we solve the following problem

$$\gamma_{w,k} = \arg \max_{\gamma_w} Q_2(\gamma_w, \gamma_{w,k-1}), \quad (33)$$

and the optimal estimation of γ_w is obtained as

$$\gamma_{w,k} = \left(\frac{1}{K_p} \|\mathbf{y}_m - \mathbf{W} \hat{\mathbf{h}}_{2,k}\|^2 + \frac{1}{K_p} \gamma_{w,k-1}^{-1} \sum_{n=1}^R \left(\frac{|s_n|^2}{|s_n|^2 + \gamma_{w,k-1}^{-1} |s_n|^2} \right) \right)^{-1} \quad (34)$$

where $\hat{\mathbf{h}}_{2,k}$ is given in (22). Detailed derivation procedure is found in Appendix C.

Last, initialization of the three parameters γ_w , λ , and γ_h , is necessary for the operation of the EM based

iterative parameter estimation. The initial value of γ_w is set as [36]

$$\gamma_{w,0} = \frac{(1 + \zeta)K_p}{\|\mathbf{y}_m\|_F^2} \quad (35)$$

where ζ as the signal-to-noise ratio (SNR) can be estimated from observation data or is just heuristically set. A heuristic initial value for the normalized sparsity, λ , has been suggested as $\lambda_0 = 0.95$. The initial value for γ_h can be set as [36]

$$\gamma_{h,0} = \frac{\|\mathbf{W}\|_F^2 \lambda_0}{\|\mathbf{y}_m\|_F^2 - K_p \gamma_{w,0}^{-1}} \quad (36)$$

The procedure of EM-VAMP channel estimation is finally summarized in Algorithm 1.

Algorithm 1: EM-VAMP Channel Estimation

Input: The measurement matrix in form of SVD decomposition $\mathbf{W} = \mathbf{U}\mathbf{S}\mathbf{V}^H$, and the observation vector \mathbf{y}_m .

Initialization: Set $\mathbf{r}_{1,1} = \mathbf{0}$, $\gamma_{1,1} = 1$, $\lambda_0 = 0.95$, and $\gamma_{w,0}$ and $\gamma_{h,0}$ according to (35) and (37).

Set the maximum number of iterations K_{\max} and stopping threshold ξ_T ;

for $k = 1, 2, \dots, K_{\max}$ **do**

$$\begin{aligned} \pi_k(i) &= \left(1 + \frac{(1-\lambda_{k-1})\mathcal{CN}(r_{1,k}(i);0,\gamma_{1,k}^{-1})}{\lambda_{k-1}\mathcal{CN}(r_{1,k}(i);0,(\gamma_{1,k}^{-1}+\gamma_{h,k-1}^{-1}))} \right)^{-1} \\ \hat{\mathbf{h}}_{1,k} &= \boldsymbol{\pi}_k \odot \frac{\gamma_{1,k}\mathbf{r}_{1,k}}{\gamma_{1,k}+\gamma_{h,k-1}}, \quad \alpha_{1,k} = \left\langle \boldsymbol{\pi}_k \frac{\gamma_{1,k}}{\gamma_{1,k}+\gamma_{h,k-1}} \right\rangle, \quad \nu_k = \frac{1}{\gamma_{1,k}+\gamma_{h,k-1}} \\ \mathbf{r}_{2,k} &= \frac{(\hat{\mathbf{h}}_{1,k}-\alpha_{1,k}\mathbf{r}_{1,k})}{1-\alpha_{1,k}}, \quad \gamma_{2,k} = \gamma_{1,k} \frac{1-\alpha_{1,k}}{\alpha_{1,k}} \\ \lambda_k &= \frac{1}{NL} \sum_{i=1}^{NL} \pi_k(i), \quad \gamma_{h,k} = \left(\frac{1}{\lambda_k NL} \sum_{i=1}^{NL} \pi_k(i) (|\mu_k(i)|^2 + \nu_k) \right)^{-1} \\ \mathbf{d}_k &= (\gamma_{w,k-1}\mathbf{S}^H\mathbf{S} + \gamma_{2,k}\mathbf{I})^{-1}, \quad \tilde{\mathbf{y}}_m = \gamma_{w,k-1}\mathbf{S}^H\mathbf{y}_m \\ \hat{\mathbf{h}}_{2,k} &= \mathbf{V}\mathbf{d}_k(\tilde{\mathbf{y}}_m + \gamma_{2,k}\mathbf{V}^H\mathbf{r}_{2,k}), \quad \alpha_{2,k} = \frac{1}{R} \sum_n \frac{\gamma_{2,k}}{\gamma_{w,k-1}s_n^2 + \gamma_{2,k}} \text{ with } s_n = [\mathbf{S}]_{nn} \\ \mathbf{r}_{1,k+1} &= \frac{(\hat{\mathbf{h}}_{2,k}-\alpha_{2,k}\mathbf{r}_{2,k})}{1-\alpha_{2,k}}, \quad \gamma_{1,k+1} = \gamma_{2,k} \frac{1-\alpha_{2,k}}{\alpha_{2,k}} \\ \gamma_{w,k} &= \left(\frac{1}{K_p} \|\mathbf{y}_m - \mathbf{W}\hat{\mathbf{h}}_{2,k}\|^2 + \frac{1}{K_p} \gamma_{w,k-1}^{-1} \sum_{n=1}^R \left(\frac{|s_n|^2}{|s_n|^2 + \gamma_{w,k-1}^{-1}|s_n|^2} \right) \right)^{-1} \\ \text{if } \|\mathbf{r}_{1,k+1} - \mathbf{r}_{1,k}\|_2^2 &\leq \xi_T \|\mathbf{r}_{1,k+1}\|_2^2 \\ &\quad \text{break.} \end{aligned}$$

end if

end

Output: $\hat{\mathbf{h}}_{1,K_f}$ where K_f is the actual number of iterations executed.

C. Complexity Analysis and Comparison

In this subsection, we analyze the computational complexity of the proposed EM-VAMP-CE scheme and compare it with those of existing schemes, including the LS, LMMSE, OMP, and SBL CEs. It is noted existing SBL CE [23] adopts a prior probability model in which channel taps follow independent Gaussian distributions with different variance. Such a model is more accurate, but involves a large number (proportional to the channel length) of hyperparameters. The complexity is measured in the number of complex multiplications (CMs). For convenience, a division operation is treated as a multiplication operation, and all the addition operations are excluded for their low computation cost [1]. As the complexity of most schemes is related to the choice of pilot sequences, both cases of orthogonal and non-orthogonal pilot sequences are investigated. In the case of non-orthogonal pilot sequences, the SVD $\mathbf{W} = \mathbf{U}\mathbf{S}\mathbf{V}^H$ is used for LS, LMMSE, EM-VAMP CEs to reduce complexity and the complexity of the SVD is not included. For the EM-VAMP-CE, the complexity of EM-based parameter estimation is much lower than the VAMP, thus is not included.

The complexity comparisons are listed in Table I, where K_h , K_f and K_s are the sparse level of $\underline{\mathbf{h}}_m$, the iteration number of the EM-VAMP-CE, and the number of iterations for the SBL-CE, respectively. Clearly, use of orthogonal pilot sequences leads to complexity saving for all but the OMP CEs. In the case of non-orthogonal pilot sequences, the EM-VAMP-CE has a much lower complexity than the SBL-CE.

TABLE I
COMPLEXITY COMPARISON (NUMBER OF CMS)

CE methods	Non-orthogonal pilot sequences	Orthogonal pilot sequences
LS	$\mathcal{O}(MN_p^2 + MN^2L^2)$	$\mathcal{O}(MNK_pL)$
LMMSE	$\mathcal{O}(MN_p^2 + MN^2L^2)$	$\mathcal{O}(MNK_pL)$
OMP	$\mathcal{O}(MN_p^2K_h + \frac{MK_h^3}{3})$	$\mathcal{O}(MN_p^2K_h + \frac{MK_h^3}{3})$
SBL	$\mathcal{O}(\frac{MN^3K_sL^3}{2} + 2MN^2K_sL^2K_p)$	$\mathcal{O}(MNK_sK_pL)$
EM-VAMP	$\mathcal{O}(MN^2K_fL^2)$	$\mathcal{O}(MNK_fK_pL)$

IV. SIMULATION RESULTS

In this section, we study the performance of the proposed EM-VAMP-CE through simulations. A 2×6 MIMO OFDM UWA communication system is considered. The twelve subchannels are taken from the

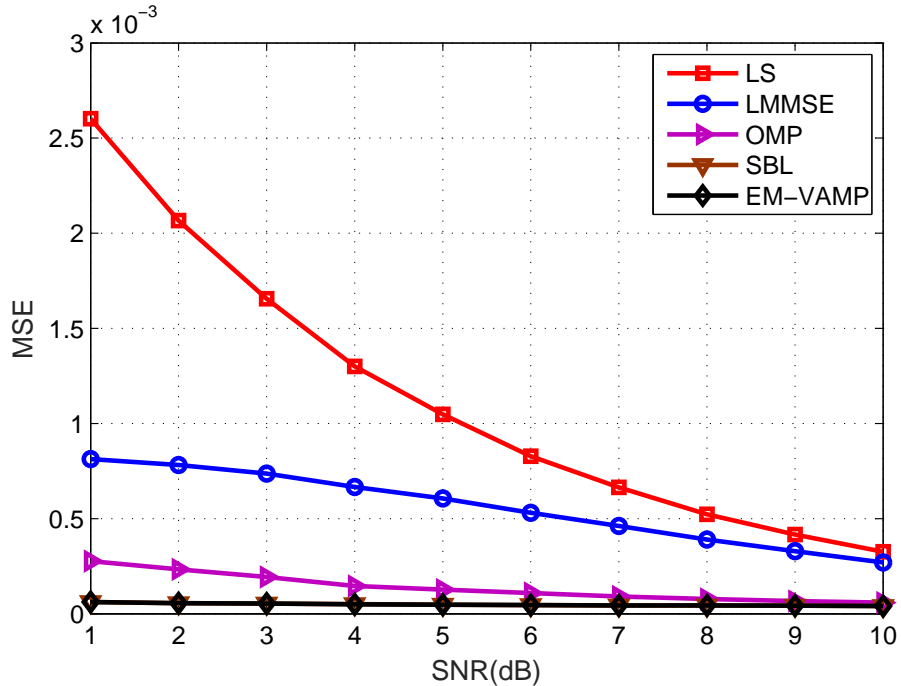


Fig. 2. Comparison of channel estimation MSE at different SNRs.

SPACE08 experiment [37], and have the same length of $L = 100$. Each OFDM block contains $K = 1024$ subcarriers including $K_d = 768$ data subcarriers and $K_p = 256$ equally-spaced pilot subcarriers for channel estimation. The pilot sequences across the two transducers are orthogonal to each other [33]. We evaluate the performance of LS, LMMSE, OMP, SBL, and EM-VAMP CEs in terms of the channel estimation mean square error (MSE).

The MSE comparison is shown in Fig. 2. From the figure, the EM-VAMP-CE and SBL-CE achieve similar channel estimation accuracy that is higher than the LS, LMMSE, and OMP CEs.

V. EXPERIMENTAL RESULTS

The proposed EM-VAMP-CE has also been tested by experimental data collected in two independent UWA communication experiments: XM16 and SPACE08. The results are presented in Section V-A and Section V-B, respectively.

A. The XM16 Experiment

This experiment was conducted at the Wuyuan Bay, Xiamen, China, in Dec. 2016. It was a multichannel communication with four hydrophone elements on the receiver side. The carrier frequency was 16 kHz and the bandwidth was 4 kHz. A rate- $\frac{1}{2}$ LDPC channel code was adopted. Every transmission packet

consisted of 6 OFDM blocks each having $K = 1280$ subcarriers, among which $K_d = 1024$ were data subcarriers, $K_p = 160$ were equally-spaced pilot subcarriers, and 96 were null subcarriers. The channel length was measured as $L = 150$.

TABLE II
THREE SETS OF PARAMETER INITIALIZATIONS.

Hyperparameter	Set Index	1	2	3
	λ		0.95	0.75
γ_h		298.7	200	100
γ_w		86.4	60	20

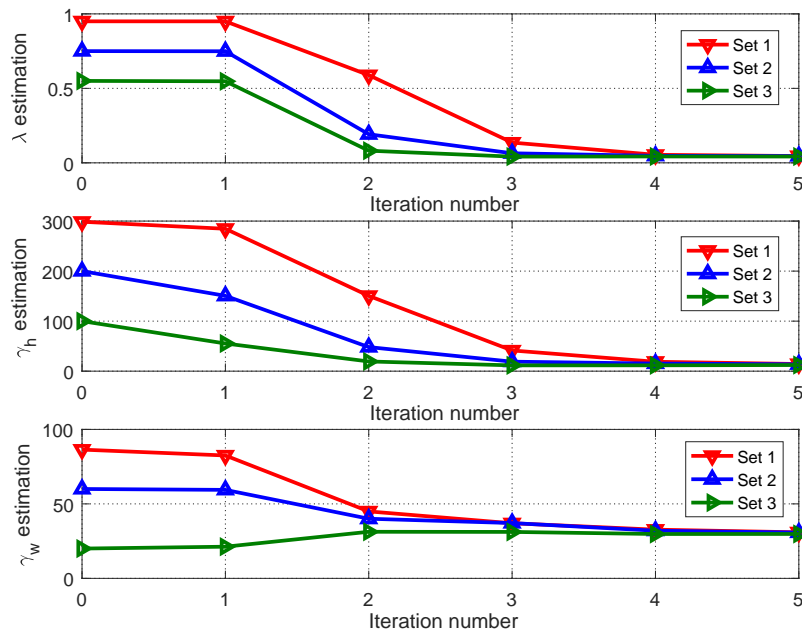


Fig. 3. Evolution of the parameter estimations.

First, we demonstrate the learning of the parameters: λ , γ_h , and γ_w . Three sets of initial values, as listed in Table II, were adopted to study the impact of initialization on the EM-based parameter estimation. The first set was obtained according to the suggested initialization introduced at the end of Section. III-B. Evolutions of the parameter estimations over EM iterations are shown in Fig. 3. Clearly, all three parameter estimations converge to almost identical values in four iterations, despite their initial settings. The insensitivity to initialization is desirable for practical use. The converged sparsity rate λ

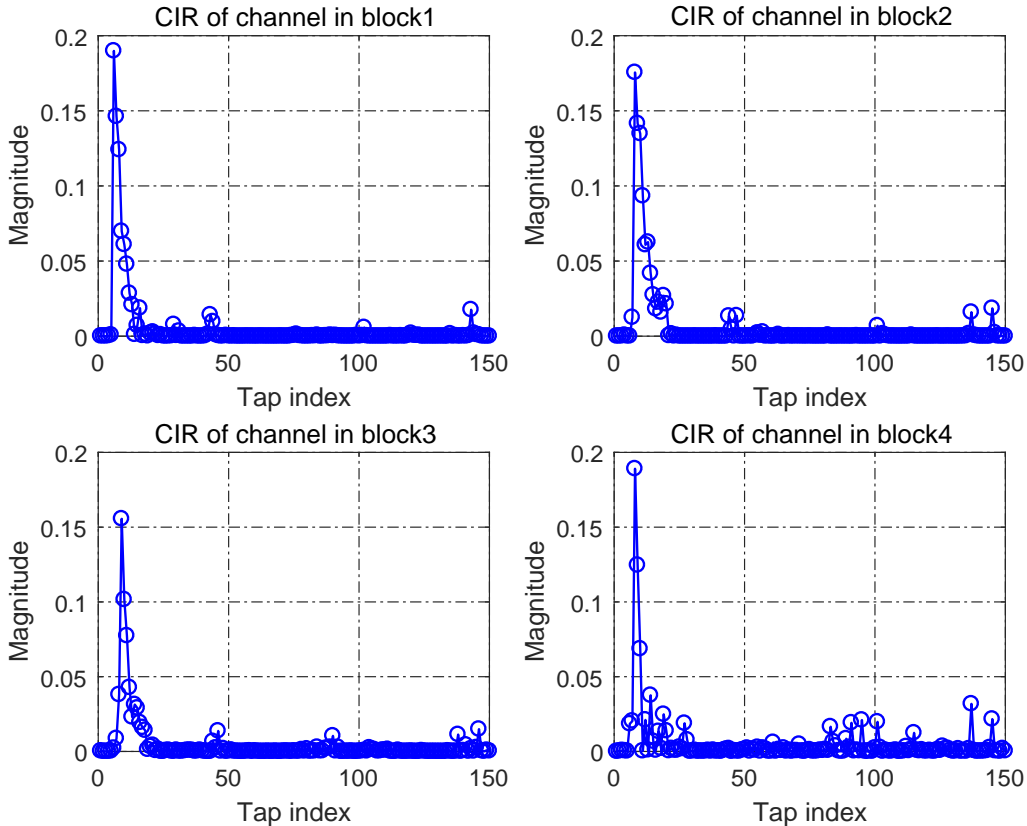
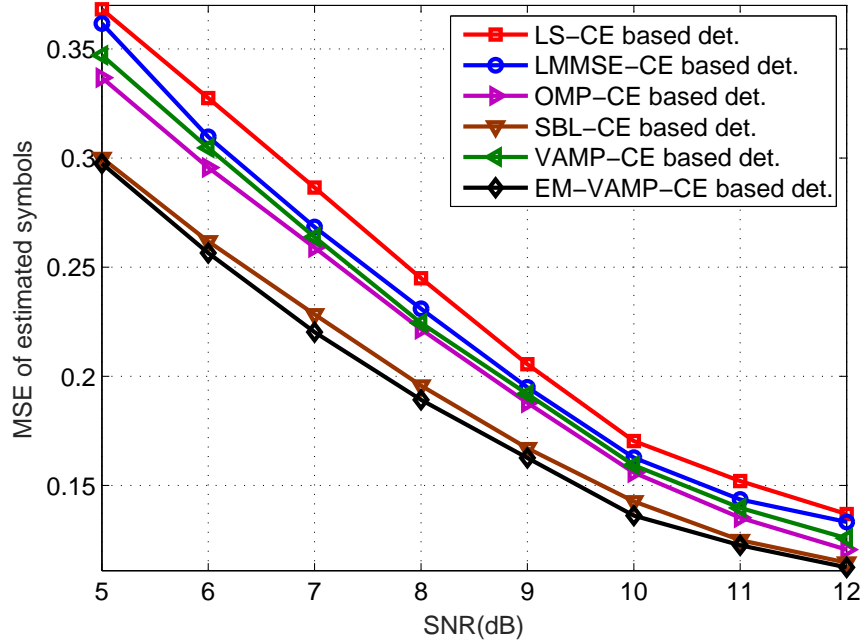


Fig. 4. Estimated channel impulse responses via EM-VAMP-CE for four blocks (XM16 experiment).

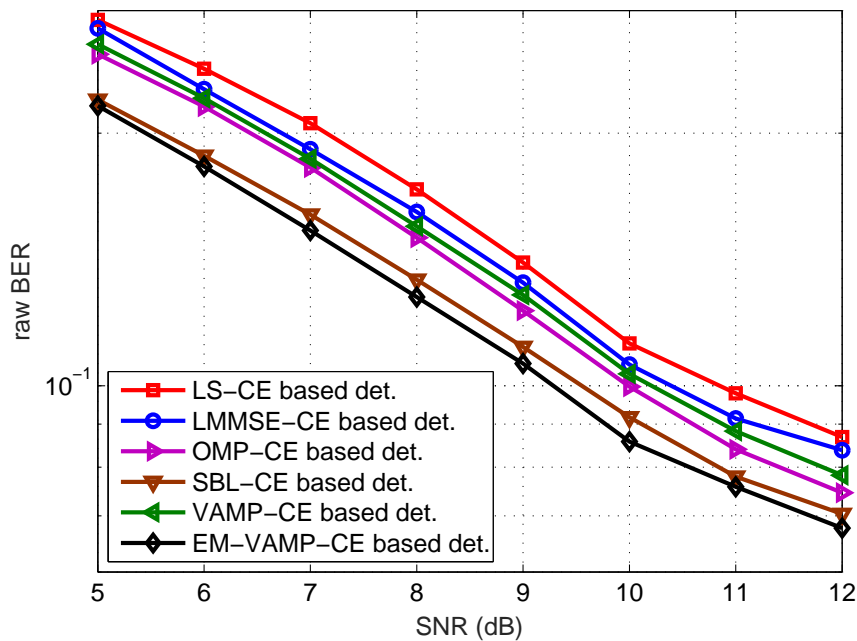
is about 0.05, indicating the underlying channel is very sparse. This is corroborated by the estimated channels of four OFDM blocks on the first receive hydrophone, demonstrated in Fig. 4.

Next, performance of the proposed EM-VAMP-CE is presented and compared with estimations based on LS, LMMSE, OMP [38], and SBL [16] algorithms. The VAMP CE with predetermined hyperparameters (which are set according to the discussion at the end of Section. III-B) was also investigated. The empirical settings are also used to initialize the EM-VAMP-CE. As the real channel is unknown, the MSE of estimated symbols and raw bit error rate (BER), that is the bit error rate before decoding, were adopted as the performance metrics. The SNR of the originally received data is about 20 dB. To enable an investigation under different SNR levels, artificial Gaussian noise was added to achieve an SNR range of 5-12 dB. The performance comparison was shown in Fig. 5, where the EM-VAMP-CE outperforms all other CEs.

Last, we investigate the impact of pilot overhead on the channel estimation performance. According to [1], the minimum number of pilots required by the LS channel estimation is equal to the channel length $L = 150$, so as to avoid an under-determined problem. Attributed to the channel sparsity, however, sparsity-aware algorithms work decently even with less pilots. Therefore, we focused on the case where



(a) MSE of estimated symbols comparison at different SNRs.



(b) Raw BER comparison at different SNRs.

Fig. 5. MSE of estimated symbols and raw BER comparisons (XM16 experiment).

the number of pilots is less than 150. The results are shown in Fig. 6, where the SNR is 20dB and the raw BER is used as the performance metric. From the figure, all but the LS CEs work properly. The EM-VAMP-CE consistently outperforms all estimation methods except for the SBL-CE, when the number of pilots goes from 115 to 145. The LS channel estimation completely failed, due to insufficient pilots.

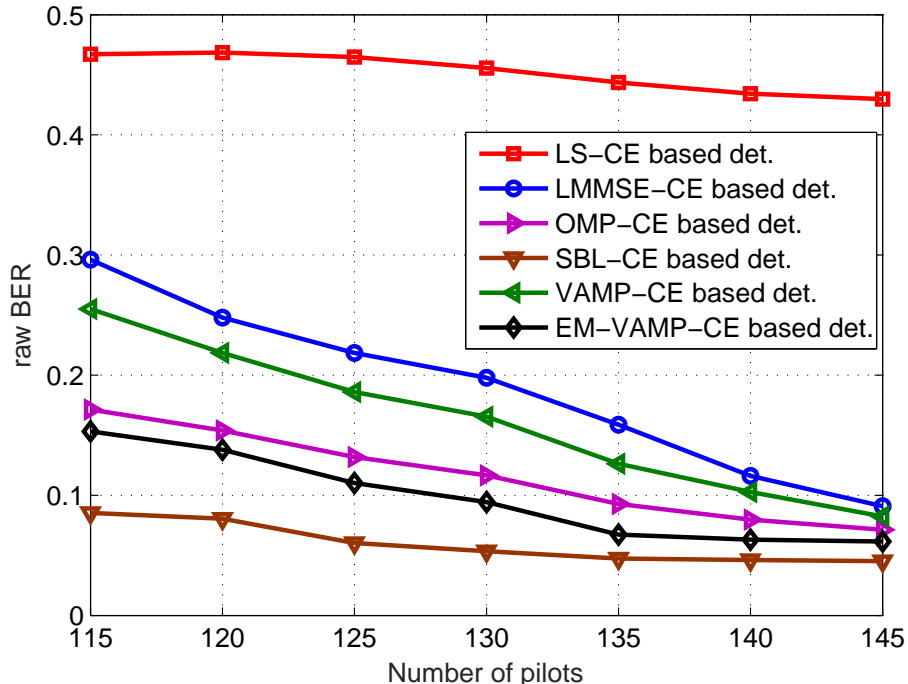


Fig. 6. Raw BER comparison with different number of pilot symbols (XM16 experiment).

B. The SPACE08 Experiment

The second experiment was performed near Martha’s Vineyard, Edgartown, MA, in 2008 [37]. The carrier frequency was 13 kHz and the occupied bandwidth was 9.7656 kHz. The QPSK modulation and a rate- $\frac{1}{2}$ convolutional channel code were adopted. The transmit equipment consisted of four transducers and the receive equipment consisted of twelve hydrophones. Experimental results for a 2×6 MIMO transmission are discussed in the following. Each transmission packet consisted of 8 QPSK blocks per transducer. Each block carried $K = 1024$ symbols with $K_p = 256$ being pilots. Non-orthogonal pilot sequences were adopted across the two transducers. In total, four received packets were processed. The lengths of all subchannels were measured within 100, and the SNR on each hydrophone was about 10 dB.

We start with investigating the effectiveness of the EM-based parameter estimation. We focus on the estimation of γ_w or equivalently, the SNR on the receiver side. The reason is that the SNR can be directly estimated with received time-domain signal, attributed to the gaps inserted among OFDM blocks. The time-domain direct estimation can be used as a reference. In Fig. 7, the SNR estimations on six receive hydrophones were compared. One can see that at convergence, the estimation via the EM algorithm is close to that estimated from the time series directly.

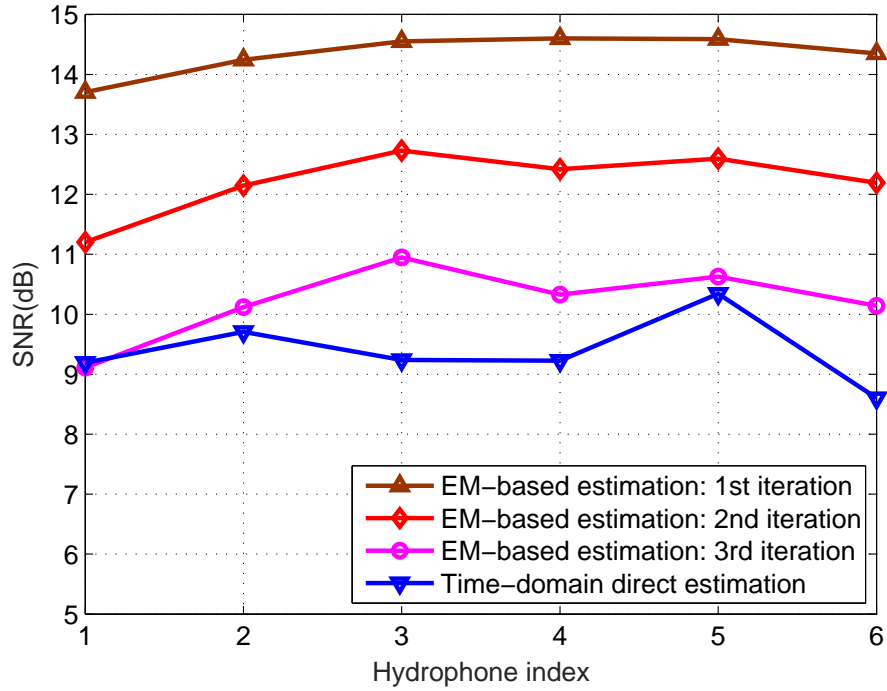


Fig. 7. A comparison of the SNR estimations (SPACE08 experiment).

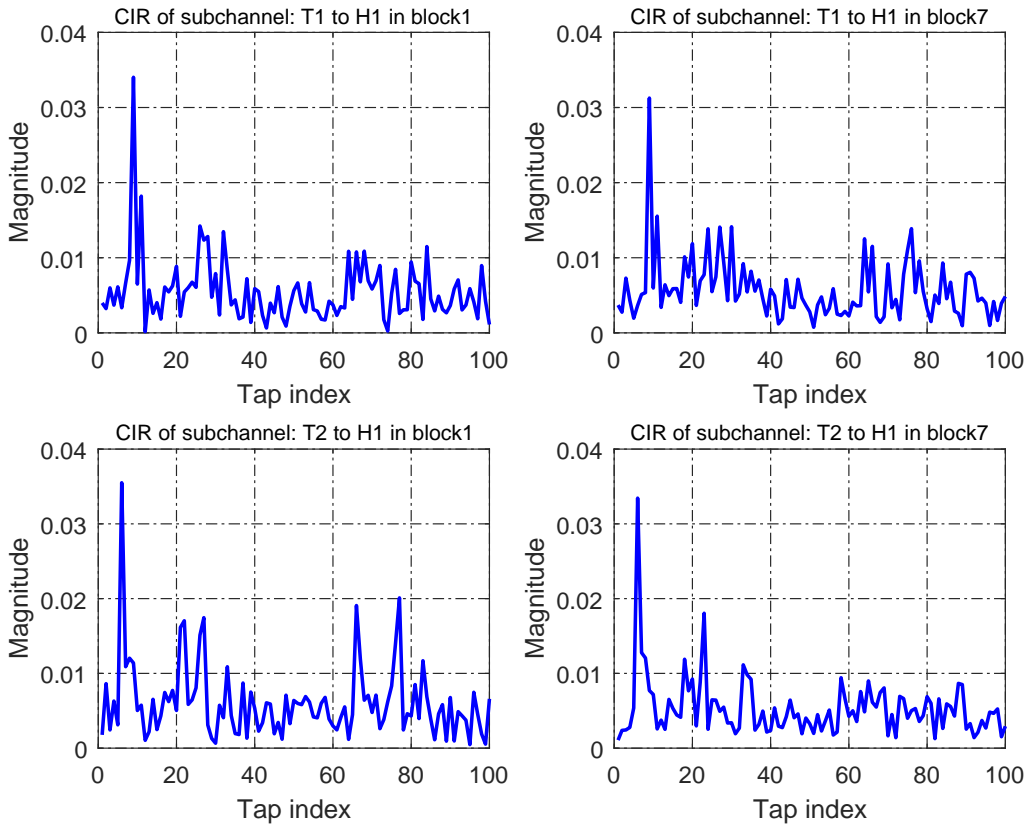


Fig. 8. The estimated channel impulse responses via EM-VAMP-CE (SPACE08 experiment).

The sparsity rate estimation for this experiment was about 0.2, indicating the underlying channel is less sparse compared with that of the previous XM16 experiment. In Fig. 8, examples of estimated subchannels between transducers 1,2 (denoted by T1 and T2) and hydrophone 1 (denoted as H1) for blocks 1 and 7, are shown.

The channel estimation results are next discussed. The comparison of symbol MSE and raw BER is shown in Fig. 9, where the number of used pilot symbols was 256. From the figure, the EM-VAMP-CE outperforms the LS, LMMSE, OMP, and VAMP CEs. Compared with the SBL-CE, it is inferior in performance but has a complexity that is three magnitude lower for this particular experiment.

For a MIMO transmission with N transducers, the minimum number of pilots is NL for the LS CE [1]. Therefore we focused on the case where the number of pilots is less than 200. The raw BER comparison among different CE methods at different number of pilots, is shown in Fig. 10. Again, the EM-VAMP-CE achieves a performance only second to the SBL-CE.

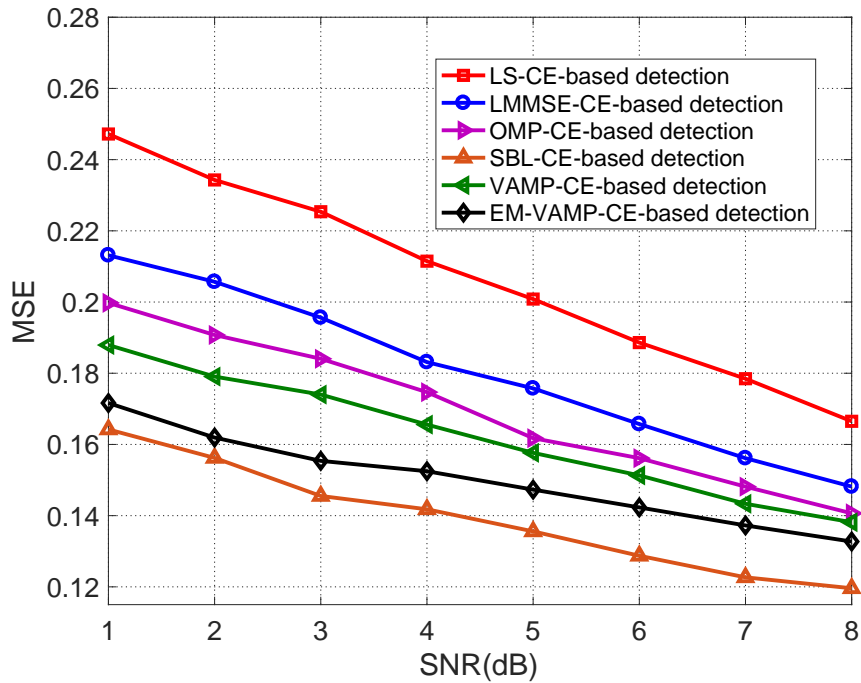
VI. CONCLUSION

In this paper, we proposed a new channel estimation scheme for MIMO OFDM underwater acoustic communications. It employed the VAMP algorithm to achieve approximate MMSE estimation of the channel. To determine the hyperparameters involved in the estimation, the EM algorithm was used. The proposed EM-VAMP channel estimation outperforms existing methods based on LS, LMMSE, OMP, as well as VAMP with predefined superparameters, according to simulation and experimental results. Even though it is slightly inferior to the SBL-CE in performance, it has a much lower complexity especially for a MIMO transmission employing non-orthogonal pilot sequences.

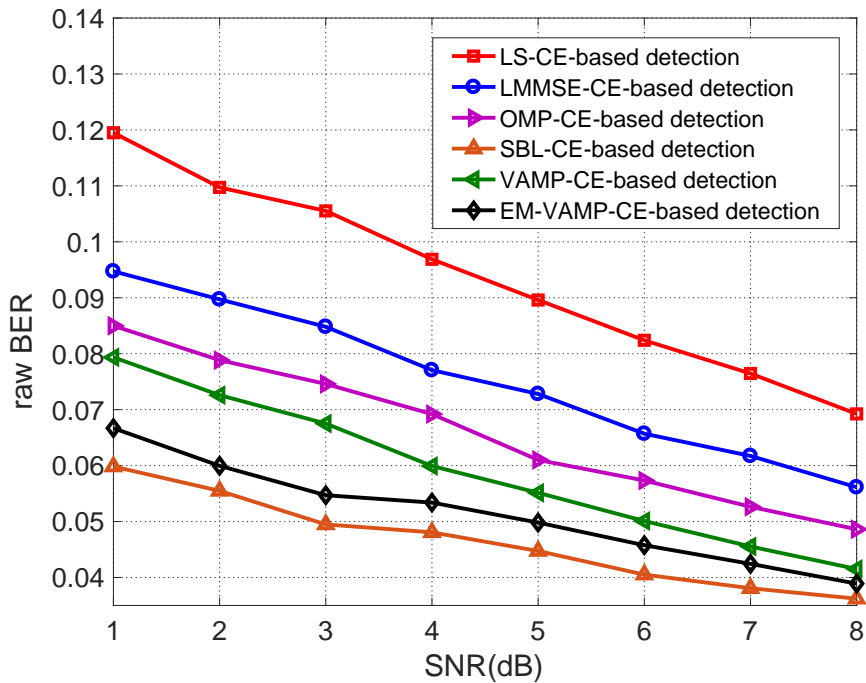
APPENDIX A

Plugging (4) into (7), one gets

$$\begin{aligned}
b_1(h_1(i)|r_{1,k}(i), \gamma_{1,k}, \boldsymbol{\theta}_1) &= \frac{\mathcal{CN}(h_1(i); r_{1,k}(i), \gamma_{1,k}^{-1})p(h_1(i); \boldsymbol{\theta}_1)}{\int \mathcal{CN}(h_1(i); r_{1,k}(i), \gamma_{1,k}^{-1})p(h_1(i); \boldsymbol{\theta}_1)dh_1(i)} \\
&= \frac{\mathcal{CN}(h_1(i); r_{1,k}(i), \gamma_{1,k}^{-1})((1 - \lambda)\delta(h_1(i)) + \lambda\mathcal{CN}(h_1(i); 0, \gamma_h^{-1}))}{(1 - \lambda)\mathcal{CN}(0; r_{1,k}(i), \gamma_{1,k}^{-1}) + \lambda\mathcal{CN}(0; r_{1,k}(i), (\gamma_{1,k}^{-1} + \gamma_h^{-1}))} \\
&= \frac{(1 - \lambda)\mathcal{CN}(0; r_{1,k}(i), \gamma_{1,k}^{-1})\delta(h_1(i))}{(1 - \lambda)\mathcal{CN}(0; r_{1,k}(i), \gamma_{1,k}^{-1}) + \lambda\mathcal{CN}(0; r_{1,k}(i), (\gamma_{1,k}^{-1} + \gamma_h^{-1}))} + \\
&\quad \frac{\lambda\mathcal{CN}(0; r_{1,k}(i), (\gamma_{1,k}^{-1} + \gamma_h^{-1}))\mathcal{CN}(h_1(i); \mu_k(i), \nu_k)}{(1 - \lambda)\mathcal{CN}(0; r_{1,k}(i), \gamma_{1,k}^{-1}) + \lambda\mathcal{CN}(0; r_{1,k}(i), (\gamma_{1,k}^{-1} + \gamma_h^{-1}))} \\
&= (1 - \pi_k(i))\delta(h_1(i)) + \pi_k(i)\mathcal{CN}(h_1(i); \mu_k(i), \nu_k)
\end{aligned} \tag{37}$$



(a) The symbol MSE comparison at different SNRs.



(b) The raw BER comparison at different SNRs.

Fig. 9. The symbol MSE and raw BER comparisons at different SNRs (SPACE08 experiment).

where $\mu_k(i)$ and ν_k are defined in (10) and (11).

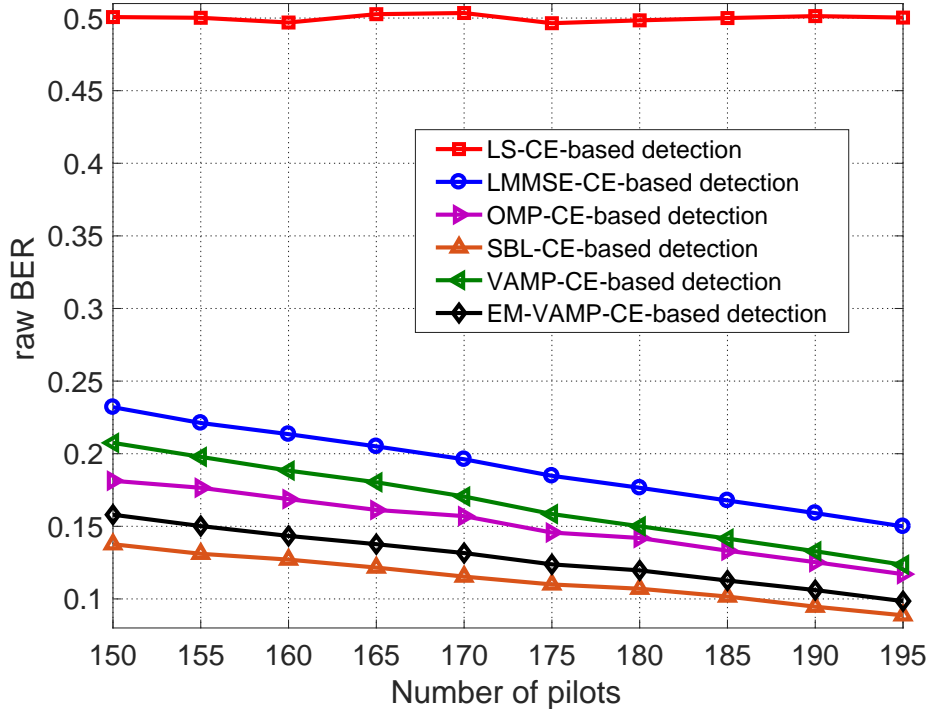


Fig. 10. The raw BER comparison under different number of pilot symbols (SPACE08 experiment).

APPENDIX B

We take the first derivative of $Q_1(\boldsymbol{\theta}_1, \boldsymbol{\theta}_{1,k-1})$ in (28) with respect to λ and set it to zero, that is

$$\begin{aligned}
\frac{\partial Q_1(\boldsymbol{\theta}_1, \boldsymbol{\theta}_{1,k-1})}{\partial \lambda} &= \frac{\partial}{\partial \lambda} \int \ln(p(\underline{\mathbf{h}}_m; \boldsymbol{\theta}_1) p(\mathbf{y}_m | \underline{\mathbf{h}}_m; \gamma_w)) b_1(\underline{\mathbf{h}}_m | \mathbf{r}_{1,k}, \gamma_{1,k}, \boldsymbol{\theta}_{1,k-1}) d\underline{\mathbf{h}}_m \\
&= \frac{\partial}{\partial \lambda} \int (\ln p(\underline{\mathbf{h}}_m; \boldsymbol{\theta}_1) + \ln p(\mathbf{y}_m | \underline{\mathbf{h}}_m; \gamma_w)) b_1(\underline{\mathbf{h}}_m | \mathbf{r}_{1,k}, \gamma_{1,k}, \boldsymbol{\theta}_{1,k-1}) d\underline{\mathbf{h}}_m \\
&= \frac{\partial}{\partial \lambda} \int \ln p(\underline{\mathbf{h}}_m; \boldsymbol{\theta}_1) b_1(\underline{\mathbf{h}}_m | \mathbf{r}_{1,k}, \gamma_{1,k}, \boldsymbol{\theta}_{1,k-1}) d\underline{\mathbf{h}}_m \\
&= \sum_{i=1}^{NL} \int b_1(\underline{h}_m(i) | r_{1,k}(i), \gamma_{1,k}, \boldsymbol{\theta}_{1,k-1}) \frac{\partial}{\partial \lambda} \ln p(\underline{h}_m(i); \boldsymbol{\theta}_1) d\underline{h}_m(i) = 0.
\end{aligned} \tag{38}$$

For the BG prior probability in (4), it is readily seen that

$$\frac{\partial}{\partial \lambda} \ln p(\underline{h}_m(i); \boldsymbol{\theta}_1) = \frac{\mathcal{CN}(\underline{h}_m(i); 0, \gamma_h^{-1}) - \delta(\underline{h}_m(i))}{p(\underline{h}_m(i); \boldsymbol{\theta}_1)} \tag{39}$$

$$= \begin{cases} \frac{1}{\lambda} & \underline{h}_m(i) \neq 0 \\ \frac{-1}{1-\lambda} & \underline{h}_m(i) = 0 \end{cases} \tag{40}$$

Substituting (40) into (38), it becomes evident that the neighborhood around the point $\underline{h}_m(i) = 0$ should be treated differently from the remainder of the complex space. Thus, we define the closed interval

$\mathcal{B}_\sigma \triangleq [-\sigma, \sigma]$ and its complement $\overline{\mathcal{B}}_\sigma \triangleq \mathcal{R} \setminus \mathcal{B}_\sigma$, with \mathcal{R} denoting the real space. In the limit $\sigma \rightarrow 0$, (38) can be transformed into

$$\begin{aligned} & \sum_{i=1}^{NL} \int_{|\underline{h}_m(i)| \in \overline{\mathcal{B}}_\sigma} b_1(\underline{h}_m(i) | r_{1,k}(i), \gamma_{1,k}, \boldsymbol{\theta}_{1,k-1}) d\underline{h}_m(i) \\ &= \frac{\lambda}{1-\lambda} \sum_{i=1}^{NL} \int_{|\underline{h}_m(i)| \in \mathcal{B}_\sigma} b_1(\underline{h}_m(i) | r_{1,k}(i), \gamma_{1,k}, \boldsymbol{\theta}_{1,k-1}) d\underline{h}_m(i). \end{aligned} \quad (41)$$

According to (8), (41) is equivalent to

$$\sum_{i=1}^{NL} \pi_k(i) = \frac{\lambda}{1-\lambda} \sum_{i=1}^{NL} (1 - \pi_k(i)), \quad (42)$$

based on which the optimal estimation of λ at the k -th iteration is solved as

$$\lambda_k = \frac{1}{NL} \sum_{i=1}^{NL} \pi_k(i). \quad (43)$$

Similarly, we take the first derivative of $\frac{\partial Q_1(\boldsymbol{\theta}_1, \boldsymbol{\theta}_{1,k-1})}{\partial \gamma_h}$ with respect to γ_h and set it to zero, leading to

$$\frac{\partial Q_1(\boldsymbol{\theta}_1, \boldsymbol{\theta}_{1,k-1})}{\partial \gamma_h} = \sum_{i=1}^{NL} \int b_1(\underline{h}_m(i) | r_{1,k}(i), \gamma_{1,k}, \boldsymbol{\theta}_{1,k-1}) \frac{\partial}{\partial \gamma_h} \ln p(\underline{h}_m(i); \boldsymbol{\theta}_1) d\underline{h}_m(i) = 0. \quad (44)$$

For the BG prior probability in (4), it is readily seen that

$$\frac{\partial}{\partial \gamma_h} \ln p(\underline{h}_m(i); \boldsymbol{\theta}_1) d\underline{h}_m(i) = \left(\frac{1}{\gamma_h} - |\underline{h}_m(i)|^2 \right) \frac{\lambda \mathcal{CN}(\underline{h}_m(i); 0, \gamma_h^{-1})}{p(\underline{h}_m(i); \boldsymbol{\theta}_1)} \quad (45)$$

$$= \begin{cases} \frac{1}{\gamma_h} - |\underline{h}_m(i)|^2 & \underline{h}_m(i) \neq 0 \\ 0 & \underline{h}_m(i) = 0 \end{cases} \quad (46)$$

Dividing the integration domain in (44) into \mathcal{B}_σ and $\overline{\mathcal{B}}_\sigma$ as before then plugging (46), (44) is equivalent to the following in the limit $\sigma \rightarrow 0$

$$\sum_{i=1}^{NL} \int_{|\underline{h}_m(i)| \in \overline{\mathcal{B}}_\sigma} (1 - \gamma_h |\underline{h}_m(i)|^2) b_1(\underline{h}_m(i) | r_{1,k}(i), \gamma_{1,k}, \boldsymbol{\theta}_{1,k-1}) d\underline{h}_m(i) = 0, \quad (47)$$

based on which the optimal γ_h is solved as

$$\begin{aligned} \gamma_{h,k} &= \frac{\sum_{i=1}^{NL} \lim_{\sigma \rightarrow 0} \int_{|\underline{h}_m(i)| \in \overline{\mathcal{B}}_\sigma} b_1(\underline{h}_m(i) | r_{1,k}(i), \gamma_{1,k}, \boldsymbol{\theta}_{1,k-1}) d\underline{h}_m(i)}{\sum_{i=1}^{NL} \lim_{\sigma \rightarrow 0} \int_{|\underline{h}_m(i)| \in \overline{\mathcal{B}}_\sigma} |\underline{h}_m(i)|^2 b_1(\underline{h}_m(i) | r_{1,k}(i), \gamma_{1,k}, \boldsymbol{\theta}_{1,k-1}) d\underline{h}_m(i)} \\ &= \left(\frac{1}{\lambda_k NL} \sum_{i=1}^{NL} \pi_k(i) (|\mu_k(i)|^2 + \nu_k) \right)^{-1} \end{aligned} \quad (48)$$

where the equality of (43) has been used.

APPENDIX C

We take the first derivative of $\frac{\partial Q_2(\gamma_w, \gamma_{w,k-1})}{\partial \gamma_w}$ in (32) with respect to γ_w and set it to zero, obtaining

$$\begin{aligned}
\frac{\partial Q_2(\gamma_w, \gamma_{w,k-1})}{\partial \gamma_w} &= \frac{\partial}{\partial \gamma_w} \int \ln(p(\underline{\mathbf{h}}_m; \boldsymbol{\theta}_1) p(\mathbf{y}_m | \underline{\mathbf{h}}_m; \gamma_w)) b_2(\underline{\mathbf{h}}_m | \mathbf{r}_{2,k}, \gamma_{2,k}, \gamma_{w,k-1}) d\underline{\mathbf{h}}_m \\
&= \frac{\partial}{\partial \gamma_w} \int (\ln p(\underline{\mathbf{h}}_m; \boldsymbol{\theta}_1) + \ln p(\mathbf{y}_m | \underline{\mathbf{h}}_m; \gamma_w)) b_2(\underline{\mathbf{h}}_m | \mathbf{r}_{2,k}, \gamma_{2,k}, \gamma_{w,k-1}) d\underline{\mathbf{h}}_m \\
&= \frac{\partial}{\partial \gamma_w} \int \ln(p(\mathbf{y}_m | \underline{\mathbf{h}}_m; \gamma_w)) b_2(\underline{\mathbf{h}}_m | \mathbf{r}_{2,k}, \gamma_{2,k}, \gamma_{w,k-1}) d\underline{\mathbf{h}}_m \\
&= \int b_2(\underline{\mathbf{h}}_m | \mathbf{r}_{2,k}, \gamma_{2,k}, \gamma_{w,k-1}) \frac{\partial}{\partial \gamma_w} \ln p(\mathbf{y}_m | \underline{\mathbf{h}}_m; \gamma_w) d\underline{\mathbf{h}}_m \\
&= 0.
\end{aligned} \tag{49}$$

It is easy to have

$$\begin{aligned}
\frac{\partial}{\partial \gamma_w} \ln p(\mathbf{y}_m | \underline{\mathbf{h}}_m; \gamma_w) &= \frac{\partial}{\partial \gamma_w} \ln \left(\left(\frac{\gamma_w}{\pi} \right)^{K_p} \exp(-\gamma_w \|\mathbf{y}_m - \mathbf{W}\underline{\mathbf{h}}_m\|_2^2) \right) \\
&= \frac{K_p}{\gamma_w} - \|\mathbf{y}_m - \mathbf{W}\underline{\mathbf{h}}_m\|_2^2.
\end{aligned} \tag{50}$$

Plugging (50) into (49), we solve γ_w as

$$\gamma_{w,k} = \left(\frac{1}{K_p} \int \|\mathbf{y}_m - \mathbf{W}\underline{\mathbf{h}}_m\|_2^2 b_2(\underline{\mathbf{h}}_m | \mathbf{r}_{2,k}, \gamma_{2,k}, \gamma_{w,k-1}) d\underline{\mathbf{h}}_m \right)^{-1} \tag{51}$$

$$= \left(\frac{1}{K_p} [\|\mathbf{y}_m - \mathbf{W}\hat{\mathbf{h}}_{2,k}\|_2^2 + \text{Tr}(\mathbf{W}(\gamma_{w,k-1} \mathbf{W}^H \mathbf{W} + \gamma_{2,k} \mathbf{I}) \mathbf{W}^H)] \right)^{-1} \tag{52}$$

$$= \left(\frac{1}{K_p} \|\mathbf{y}_m - \mathbf{W}\hat{\mathbf{h}}_{2,k}\|_2^2 + \frac{1}{K_p} \gamma_{w,k-1}^{-1} \sum_{n=1}^R \left(\frac{|s_n|^2}{|s_n|^2 + \gamma_{w,k-1}^{-1} |s_n|^2} \right) \right)^{-1} \tag{53}$$

where (52) has used (19). The (53) is obtained by replacing \mathbf{W} in (52) by its SVD $\mathbf{W} = \mathbf{U}\mathbf{S}\mathbf{V}^H$ for reduced complexity.

REFERENCES

- [1] J. Tao, "DFT-precoded MIMO OFDM underwater acoustic communications," *IEEE Journal of Oceanic Engineering*, vol. 43, no. 3, pp. 805–819, Jul. 2018.
- [2] R. Barazideh, S. Niknam, B. Natarajan, and A. V. Nikitin, "Intermittently nonlinear impulsive noise mitigation and doppler shift compensation in UWA-OFDM systems," *IEEE Access*, vol. 7, pp. 36 590–36 599, 2019.
- [3] G. Qiao, Z. Babar, L. Ma, and N. Ahmed, "Channel estimation and equalization of underwater acoustic MIMO-OFDM systems: A review estimation du canal et l'égalisation des systèmes MEMS-MROF acoustiques sous-marins: une revue," *Canadian Journal of Electrical and Computer Engineering*, vol. 42, no. 4, pp. 199–208, Aug. 2019.

- [4] J. Huang, X. Hu, F. Xu, W. Lei, and W. Weng, "Implement of channel estimation for OFDM communication system under UWA channel," in *Proc. 2008 International Conference on Communications, Circuits and Systems*, 2008, pp. 57–61.
- [5] Y. Zhang, H. Sun, F. Xu, and D. Wang, "OFDM transform-domain channel estimation based on MMSE for underwater acoustic channels," in *Proc. 2008 2nd International Conference on Anti-counterfeiting, Security and Identification*, 2008, pp. 177–181.
- [6] X. Huang and V. B. Lawrence, "OFDM with pilot aided channel estimation for time-varying shallow water acoustic channels," in *Proc. 2010 International Conference on Communications and Mobile Computing*, vol. 2, 2010, pp. 442–446.
- [7] Y. Wang, "Underwater acoustic channel estimation for pilot based OFDM," in *Proc. 2011 IEEE International Conference on Signal Processing, Communications and Computing (ICSPCC)*, 2011, pp. 1–5.
- [8] W. Li and J. C. Preisig, "Estimation of rapidly time-varying sparse channels," *IEEE Journal of Oceanic Engineering*, vol. 32, no. 4, pp. 927–939, Oct. 2007.
- [9] F. Yu, D. Li, Q. Guo, Z. Wang, and W. Xiang, "Block-FFT based OMP for compressed channel estimation in underwater acoustic communications," *IEEE Communications Letters*, vol. 19, no. 11, pp. 1937–1940, Nov. 2015.
- [10] P. Chen, Y. Rong, S. Nordholm, Z. He, and A. J. Duncan, "Joint channel estimation and impulsive noise mitigation in underwater acoustic OFDM communication systems," *IEEE Transactions on Wireless Communications*, vol. 16, no. 9, pp. 6165–6178, Sept. 2017.
- [11] Z. Wang, Y. Li, C. Wang, D. Ouyang, and Y. Huang, "A-OMP: an adaptive OMP algorithm for underwater acoustic OFDM channel estimation," *IEEE Wireless Communications Letters*, vol. 10, no. 8, pp. 1761–1765, Aug. 2021.
- [12] J. Huang, C. R. Berger, S. Zhou, and J. Huang, "Comparison of basis pursuit algorithms for sparse channel estimation in underwater acoustic OFDM," in *Proc. OCEANS'10 IEEE SYDNEY*, 2010, pp. 1–6.
- [13] Y. Yin, S. Liu, G. Qiao, and Y. Yang, "OFDM demodulation using virtual time reversal processing in underwater acoustic communications," *Journal of Computational Acoustics*, vol. 23, no. 04, p. 1540011, Dec. 2015.
- [14] C. R. Berger, S. Zhou, J. C. Preisig, and P. Willett, "Sparse channel estimation for multicarrier underwater acoustic communication: from subspace methods to compressed sensing," *IEEE Transactions on Signal Processing*, vol. 58, no. 3, pp. 1708–1721, Mar. 2010.
- [15] M. E. Tipping, "Sparse bayesian learning and the relevance vector machine," *Journal of Machine Learning Research*, vol. 1, no. 3, pp. 211–244, Jun. 2001.
- [16] D. Wipf and B. Rao, "Sparse bayesian learning for basis selection," *IEEE Transactions on Signal Processing*, vol. 52, no. 8, pp. 2153–2164, Jul. 2004.
- [17] D. L. Donoho, A. Maleki, and A. Montanari, "Message-passing algorithms for compressed sensing," *Proceedings of the National Academy of Sciences of the United States of America*, vol. 106, no. 45, pp. 18914–18919, Jul. 2009.
- [18] M. Bayati and A. Montanari, "The dynamics of message passing on dense graphs, with applications to compressed sensing," *IEEE Transactions on Information Theory*, vol. 57, no. 2, pp. 764–785, Feb. 2011.
- [19] J.-G. Kim and J.-T. Lim, "MAP-based channel estimation for MIMO-OFDM over fast rayleigh fading channels," *IEEE Transactions on Vehicular Technology*, vol. 57, no. 3, pp. 1963–1968, May. 2008.
- [20] R. Prasad, C. R. Murthy, and B. D. Rao, "Joint approximately sparse channel estimation and data detection in OFDM systems using sparse bayesian learning," *IEEE Transactions on Signal Processing*, vol. 62, no. 14, pp. 3591–3603, Jul. 2014.
- [21] X. Wu, L. Gu, W. Wang, and X. Gao, "Pilot design and AMP-based channel estimation for massive MIMO-OFDM uplink transmission," in *Proc. 2016 IEEE 27th Annual International Symposium on Personal, Indoor, and Mobile Radio Communications (PIMRC)*, 2016, pp. 1–7.
- [22] E. Panayirci, M. T. Altabaa, M. Uysal, and H. V. Poor, "Sparse channel estimation for OFDM-based underwater acoustic systems in rician fading with a new OMP-MAP algorithm," *IEEE Transactions on Signal Processing*, vol. 67, no. 6, pp. 1550–1565, Mar. 2019.

- [23] G. Qiao, Q. Song, L. Ma, S. Liu, Z. Sun, and S. Gan, "Sparse bayesian learning for channel estimation in time-varying underwater acoustic OFDM communication," *IEEE Access*, vol. 6, pp. 56 675–56 684, 2018.
- [24] S. Wang, Z. He, K. Niu, P. Chen, and Y. Rong, "New results on joint channel and impulsive noise estimation and tracking in underwater acoustic OFDM systems," *IEEE Transactions on Wireless Communications*, vol. 19, no. 4, pp. 2601–2612, Apr. 2020.
- [25] S. Wu, S. Wang, Z. He, K. Niu, and Y. Rong, "An approximate message passing algorithm for channel and impulsive noise estimation in underwater acoustic OFDM systems," in *Proc. OCEANS 2019 - Marseille*, 2019, pp. 1–5.
- [26] T.-J. Lee and Y.-C. Ko, "Channel estimation and data detection in the presence of phase noise in MIMO-OFDM systems with independent oscillators," *IEEE Access*, vol. 5, pp. 9647–9662, 2017.
- [27] X. Lv, Y. Li, Y. Wu, X. Wang, and H. Liang, "Joint channel estimation and impulsive noise mitigation method for OFDM systems using sparse bayesian learning," *IEEE Access*, vol. 7, pp. 74 500–74 510, 2019.
- [28] M. Al-Shoukairi, P. Schniter, and B. D. Rao, "A GAMP-based low complexity sparse bayesian learning algorithm," *IEEE Transactions on Signal Processing*, vol. 66, no. 2, pp. 294–308, Jan. 2018.
- [29] J. Zhu, L. Han, and X. Meng, "An AMP-based low complexity generalized sparse bayesian learning algorithm," *IEEE Access*, vol. 7, pp. 7965–7976, 2019.
- [30] S. Rangan, "Generalized approximate message passing for estimation with random linear mixing," in *Proc. 2011 IEEE International Symposium on Information Theory Proceedings*, 2011, pp. 2168–2172.
- [31] S. Rangan, P. Schniter, and A. K. Fletcher, "Vector approximate message passing," in *Proc. 2017 IEEE International Symposium on Information Theory (ISIT)*, 2017, pp. 1588–1592.
- [32] S. Rangan, P. Schniter, and A. K. Fletcher, "Vector approximate message passing," *IEEE Transactions on Information Theory*, vol. 65, no. 10, pp. 6664–6684, Oct. 2019.
- [33] I. Barhumi, G. Leus, and M. Moonen, "Optimal training design for MIMO OFDM systems in mobile wireless channels," *IEEE Transactions on Signal Processing*, vol. 51, no. 6, pp. 1615–1624, Jun. 2003.
- [34] B. Muquet, Z. Wang, G. Giannakis, M. de Courville, and P. Duhamel, "Cyclic prefixing or zero padding for wireless multicarrier transmissions?" *IEEE Transactions on Communications*, vol. 50, no. 12, pp. 2136–2148, Dec. 2002.
- [35] A. K. Fletcher and P. Schniter, "Learning and free energies for vector approximate message passing," in *Proc. 2017 IEEE International Conference on Acoustics, Speech and Signal Processing (ICASSP)*, 2017, pp. 4247–4251.
- [36] J. P. Vila and P. Schniter, "Expectation-maximization gaussian-mixture approximate message passing," *IEEE Transactions on Signal Processing*, vol. 61, no. 19, pp. 4658–4672, Oct. 2013.
- [37] J. Tao, Y. R. Zheng, C. Xiao, and T. C. Yang, "Robust MIMO underwater acoustic communications using turbo block decision-feedback equalization," *IEEE Journal of Oceanic Engineering*, vol. 35, no. 4, pp. 948–960, Oct. 2010.
- [38] J. A. Tropp and A. C. Gilbert, "Signal recovery from random measurements via orthogonal matching pursuit," *IEEE Transactions on Information Theory*, vol. 53, no. 12, pp. 4655–4666, Mar. 2007.